frontiers | Frontiers in Materials

TYPE Original Research
PUBLISHED 28 November 2023
DOI 10.3389/fmats.2023.1258222

Check for updates

OPEN ACCESS

EDITED BY
Biao Zhao,
Fudan University, China

REVIEWED BY
Houbing Huang,
Beijing Institute of Technology, China
Zhiyi Ding,
University of Shanghai for Science and Technology, China

*CORRESPONDENCE
Haifeng Wang,
wanghf@gia.cas.cn

RECEIVED 13 July 2023
ACCEPTED 13 November 2023
PUBLISHED 28 November 2023

CITATION
Liang L, Wang R, Chen D, Liu R, Ma P, Wu T and Wang H (2023), Magnetic properties of Ce-containing Pr/Nd-Fe-B sintered magnets by diffusing Nd-Dy-Al alloy.
Front. Mater. 10:1258222.
doi: 10.3389/fmats.2023.1258222

COPYRIGHT
© 2023 Liang, Wang, Chen, Liu, Ma, Wu and Wang. This is an open-access article distributed under the terms of the Creative Commons Attribution License (CC BY). The use, distribution or reproduction in other forums is permitted, provided the original author(s) and the copyright owner(s) are credited and that the original publication in this journal is cited, in accordance with accepted academic practice. No use, distribution or reproduction is permitted which does not comply with these terms.

Magnetic properties of Ce-containing Pr/Nd-Fe-B sintered magnets by diffusing Nd-Dy-Al alloy

Liwei Liang[1], Ruixiang Wang[1], Dehai Chen[1], Renhui Liu[1], Pengfei Ma[2], Tong Wu[3] and Haifeng Wang[2]*

[1]Jiang xi University of Science and Technology, Ganzhou, China, [2]Ganjiang Innovation of Academy, Chinese Academy of Science, Ganzhou, China, [3]University of Science and Technology of China, Hefei, Anhui, China

In this study, 5% wt Ce-containing sintered Pr/Nd-Ce-Fe-B magnets were processed by grain boundary diffusion (GBD) with NdxDy90-xAl10 alloy (x = 0, 10, and 20 correspond to N0, N10, and N20, respectively). After the GBD process, the coercivity of magnets increased from 1,124.7 to 1,656.4, 1,673.9, and 1,584.8 kA/m, for N0, N10, and N20, respectively. Microstructure analysis revealed continuous RE-rich intergranular phases around matrix grains, which by weakening the magnetic coupling effect between ferromagnetic matrix grains, thus, leads to coercivity improvement. N10 had the same coercivity enhancement as N0, while the Dy utilization for N10 is lower than that for N0. The SEM results showed that the inclusion of Nd leads to the formation of a network of low-melting grain boundary phases, providing channels for subsequent Dy diffusion. A $CeFe_2$ phase was found in the 5% wt Ce-containing magnet, which hindered diffusion due to its high melting point; in order to inhibit the negative impact of $CeFe_2$ and reveal the diffusion mechanism in the Ce-containing magnet, DyH3, as a diffusion source, was applied to 5% wt-Ce-containing magnets simultaneously; after the GBD process, Nd10Dy90Al10 alloy, as a diffusion source, has better coercivity enhancement than DyH3, due to the deeper diffusion of the Dy element in the Nd10Dy90Al10 diffusion.

KEYWORDS

sintered Nd/Pr-Ce-Fe-B magnet, grain boundary diffusion, microstructure, NdxDy90-xAl10 alloy, coercivity enhancement

1 Introduction

Sintered Nd-Fe-B is widely used in VCM motors, wind power generators, and driving motors (Takezawa et al., 2015; Lu et al., 2017; Liu et al., 2019; Zhou et al., 2023). The increasing demand in various applications has led to significant consumption of rare earth elements (REs). Furthermore, the scarce and expensive heavy rare earth elements Dy and Tb are being consumed in increasing amounts to satisfy the growing intrinsic-coercivity (Hcj) demands of magnets (Zeng et al., 2019; Wang et al., 2020; Jiang et al., 2022; Li et al., 2022). In contrast, the rare earth element Ce is overstocked due to its lower intrinsic magnetic properties (Shi et al., 2019; Zhang et al., 2019; Chen et al., 2020). This limits the use of Ce to low-end applications, which typically requires only small amounts of Ce. In order to increase Ce utilization, the grain boundary diffusion process (GBDP) has been employed to produce Ce-containing Nd-Fe-B magnets (Sepehri-Amin et al., 2013; Fan et al., 2018; Zeng et al., 2020). Chen et al. (2020) applied GBDP to

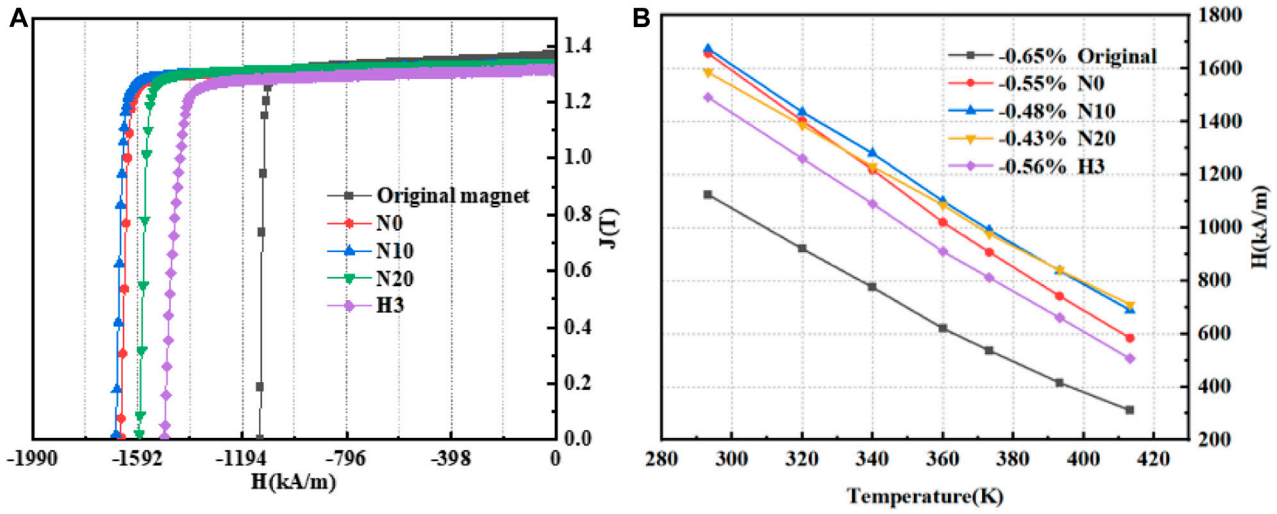

FIGURE 1
(A) Demagnetization curves of the original and GBD-processed samples. **(B)** Coefficients of coercivity β of the original and GBD-processed samples.

TABLE 1 Summary of the magnetic properties of the original and diffused samples.

Sample	Deposited Dy (wt%)	Br (T)	Hcj (kA/m)	ΔHcj (kA/m)	Hcj improvement rate (%)
Original	0	1.354	1,124.7		
N0	0.90	1.316	1,656.4	531.7	47.2
N10	0.80	1.319	1,673.9	549.2	48.8
N20	0.70	1.329	1,584.8	460.1	40.9
H3	1.00	1.303	1,490.9	366.2	32.5

a Ce-based permanent magnet with $Nd_{70}Cu_{30}$ and $Dy_{70}Cu_{30}$ eutectic alloys. The coercivity increments remained almost constant, given whatever diffusion source was used. Moreover, the thermal stability of the magnets treated with $Nd_{70}Cu_{30}$ alloy was much higher than that of the magnet treated with $Dy_{70}Cu_{30}$ alloy. A continuous grain boundary phase was observed in the magnet treated with $Nd_{70}Cu_{30}$ alloy; however, a less continuous grain boundary phase was observed in the magnet treated with $Dy_{70}Cu_{30}$ alloy. This indicates that Nd can optimize the GB distribution during GBDP. In Ce-containing magnets, a $CeFe_2$ phase is formed when the Ce proportion is above 5% in Nd-Fe-B magnets (Cui et al., 2014; Liang et al., 2014; Zhu et al., 2014; Zhu et al., 2022). This is considered to be the main factor hindering diffusion due to the high melting point of the $CeFe_2$ phase. Moreover, Du et al. (2022) used commercial N45 sintered Nd-Ce-Fe-B magnets processed by GBD with TbH_x and $Tb_{70}Fe_{30}$ alloys. The coercivity was significantly improved from 1,011.7 to 1758.4 and 1764.7 kA/m. According to Di et al. (2018), grain boundary diffusion (GBD) was applied to a sintered Nd-Fe-B magnet with Al-aided TbH_2 and TbH_2. The coercivity was enhanced from 1,092.9 to 1853.8 kA/m for Al-aided TbH_2, higher than 1771.9 kA/m of the TbH_2 GBD magnet. Microstructure analysis of the Al-aided TbH_2 processed sample showed that continuous grain boundary phases were formed and completely enveloped the grains with thin Tb-rich shells, which can be attributed to the promoted diffusion aided by Al.

Hence, this paper uses an $Nd_xDy_{90-x}Al_{10}$ alloy as a diffusion source to increase the coercivity of Ce-containing Nd-Fe-B magnets. Simultaneously, a traditional DyH_3 diffusion source was employed as a comparative sample. The influences of Nd addition on the microstructure and magnetic properties of the Ce-containing magnets were comprehensively investigated.

2 Experiment

A commercial sintered Nd-Fe-B magnet composed of $Ce_5Pr_{6.5}Nd_{19.5}M_{1.6}B_{0.92}Fe_{bal}$ (wt%, M = Cu,Co,Ga,Ti,Al) was used as the original magnet. The size of an original magnet was 10 × 10 × 5 mm, and the direction of 5 mm is the orientation direction and the diffusion direction. The original magnets were polished with an abrasive paper and cleaned with alcohol. Diffusion flakes were prepared by melt-spinning with a wheel speed of 1.3 m/s. The flakes were then nitrogen-crushed into powder with an average particle size of <17 μm. The diffusion powders were added to and mixed with alcohol, which was then used to cover the magnets on two easy planes (c-planes) homogeneously. In this work, the samples treated with $Nd_xDy_{90-x}Al_{10}$ (x = 0, 10, and 20) were marked N0, N10, and N20, respectively. In comparison, DyH_3 as the diffusion source was coated on the surface of the magnets and treated simultaneously;

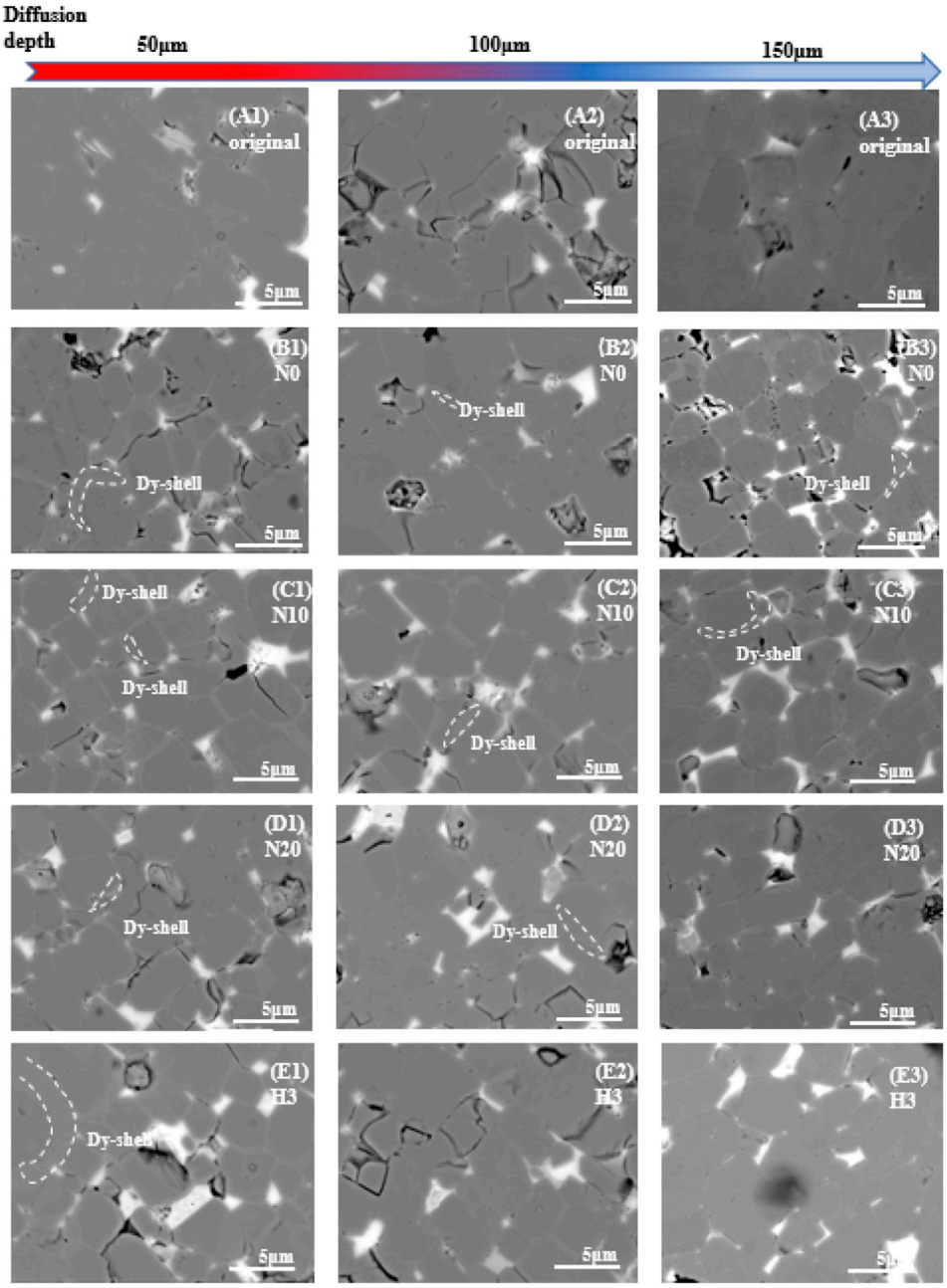

FIGURE 2
SEM images of magnets: **(A1–A3)** are original magnets, **(B1–B3)** are N0 diffused samples, **(C1–C3)** are N10 diffused samples, **(D1–D3)** are N20 diffused samples, and **(E1–E3)** are H3 diffused samples.

in this paper, it was marked as H3. In this study, 1.0 wt% by weight of the original magnet weight was coated onto the surface of the magnets. The magnets were then heat treated at 1,213.2 K for various time durations from 0 to 5 h, followed by annealing at 923.2 K for 5 h. The magnetic properties of the magnets were tested using an NIM62000C magnetometer. The microstructures of the magnets were observed using a scanning electronic microscope (SEM) (CLARA GMH), and the phase compositions were determined using an energy dispersive spectrometer (EDS). The element distribution was analyzed using an electron probe microanalyzer (EPMA-JXA-ISP100).

3 Results and discussion

Figure 1A shows the room temperature demagnetization curves of the original magnet and the diffused magnets treated at 1,213.2 K/5 h, followed by 923.2 K/5 h. The remanence (Br), intrinsic coercivity (Hcj), coercivity increment, and Dy utilization are summarized in Table 1. After diffusion, the coercivity increases from 1,124.7 kA/m to 1,656.4, 1,673.9, 1,584.8, and 1,490.9 kA/m for the N0, N10, N20, and H3 diffused magnets, respectively. The increment rates for coercivity are 47.2%, 48.8%, 40.9%, and 32.5%, respectively. The deposited Dy in N10 diffusion is 0.8% wt of the original magnet, which is lower than N0

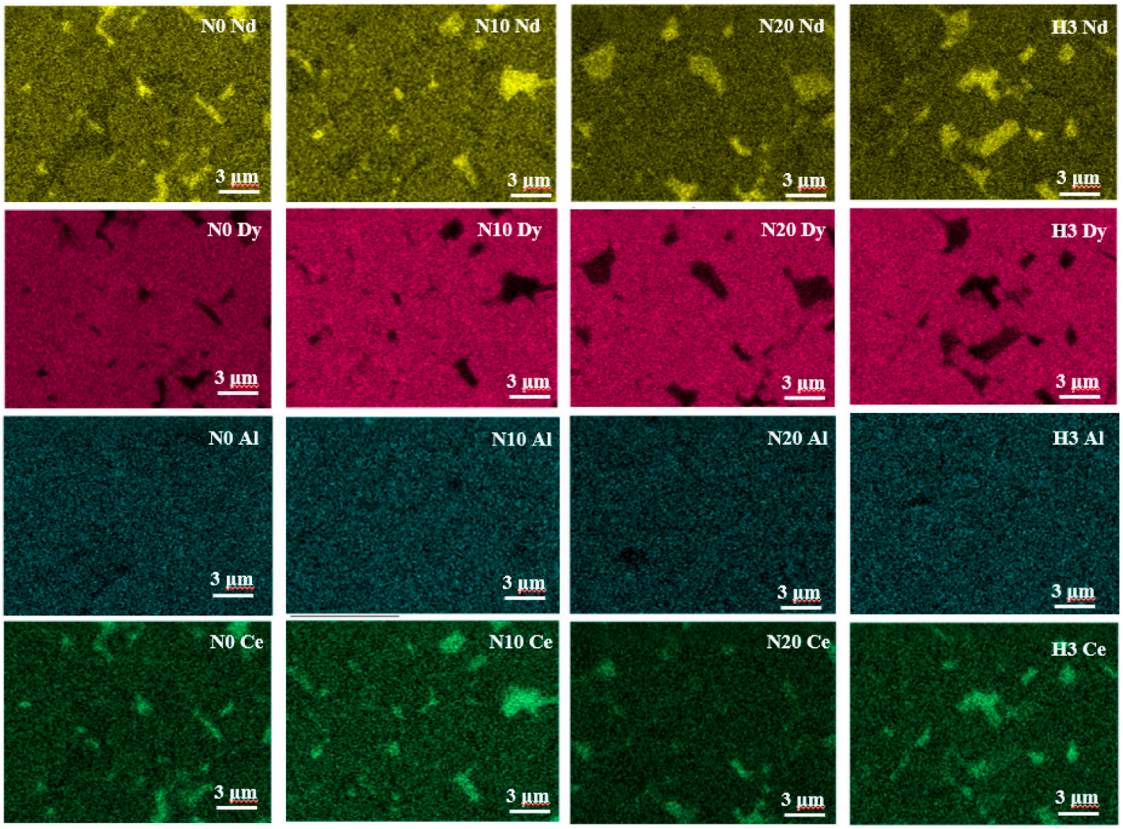

FIGURE 3
EDS images for diffused samples at a depth of 50 μm.

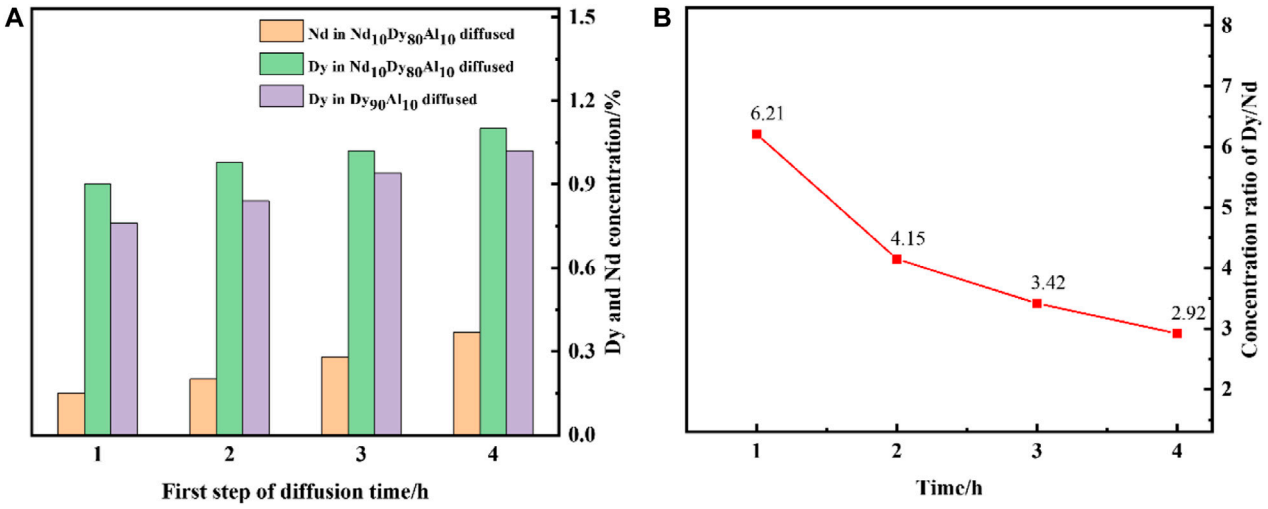

FIGURE 4
(A) Nd and Dy concentrations at a depth of 100 μm in diffused magnets. **(B)** Concentration ratio Dy/Nd at a depth of 100 μm in the $Nd_{10}Dy_{80}Al_{10}$ diffused sample. A total of 10 EDS mappings were measured in each sample to ensure the accuracy.

(0.9%wt) and H3 (1%wt), but the coercivity increment rate is higher than that of the two others. Although the coercivity increment rate for N20 diffusion is 40.9%, which is lower than N10 (48.8%), Dy is inadequate in N20 diffusion. At the same time, the remanence (Br) of diffused magnets decreases from 1.354 T to 1.316, 1.319, 1.329, and 1.303T, and N20 possesses the highest Br. The decrease in Br is most

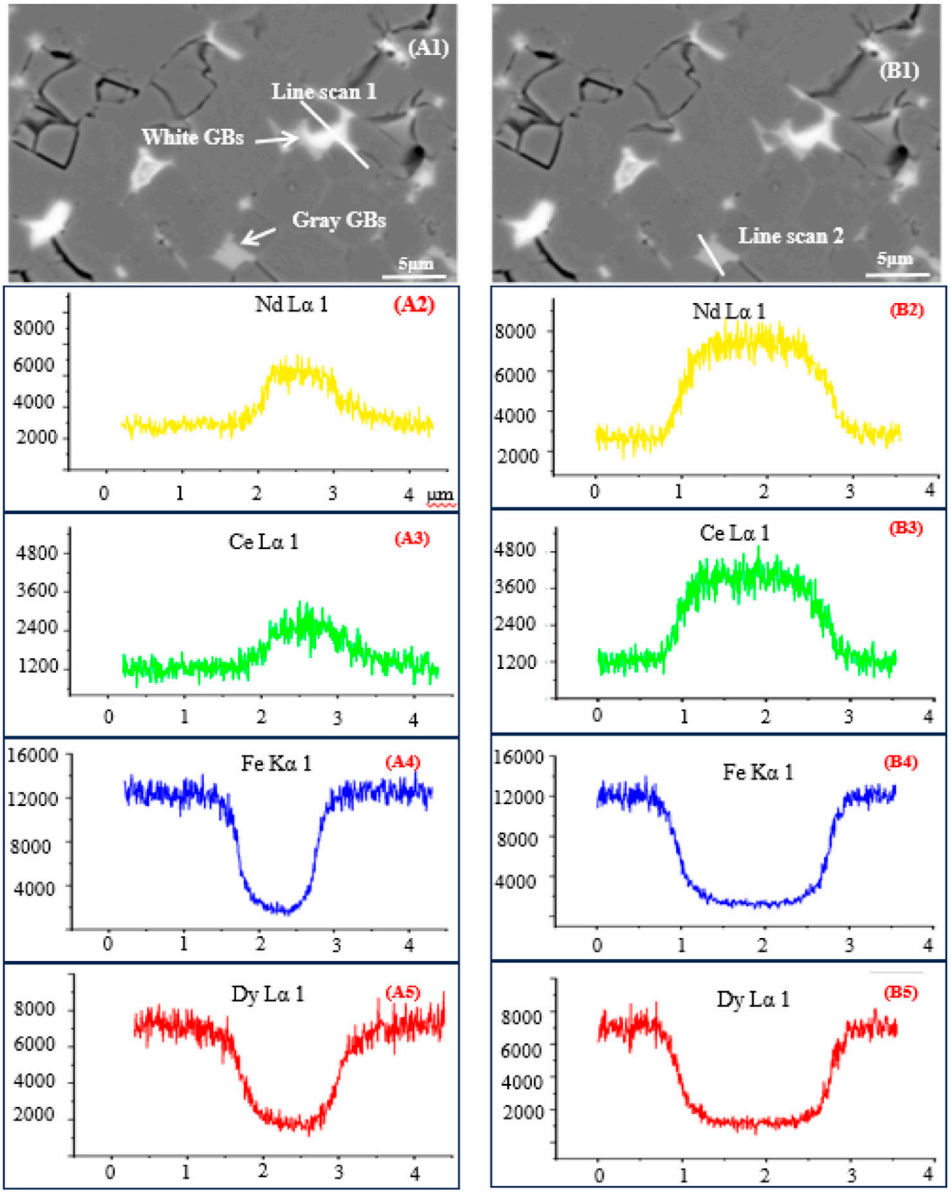

FIGURE 5
EDS line scan results for GBs of the diffused samples **(A1–A5)** for the RE-rich phase and **(B1–B5)** for the $CeFe_2$ phase.

likely caused by the substitution of Dy for Pr and Nd, as well as the increased volume fraction of non-magnetic phases in the grain boundary (Zeng et al., 2019).

Figure 1B shows the temperature coefficients of coercivity β at 280–420 K. β is usually used to measure the temperature stability of a magnet and is given by the following equation:

$$\beta = \frac{Hcj(T) - Hcj(T0)}{Hcj(T0)(T - T0)} \times 100\% \quad (1)$$

The lower the absolute value of β, the higher the temperature stability of the magnet. Figure 1B shows that the value of β improved from −0.65%/K in the original magnet to −0.55%/K, −0.48%/K, −0.43%/K, and −0.56%/K in N0, N10, N20, and H3, respectively. The enhancement in coercivity is responsible for the increased temperature stability. Moreover, the temperature stability of N20 and N10 is better than that of N0 and H3. The addition of Nd optimizes the wettability between grains and RE-rich layers, which leads to higher coercivity enhancement in N10 and N20. Furthermore, the substitution of Pr with Nd increases the temperature stability of N10 and N20 due to the forming of a high Curie temperature $Nd_2Fe_{14}B$ (585K) phase than $Pr_2Fe_{14}B$ (565K) (Zhang et al., 2019).

Figure 2 presents the back-scattered electron images of original and diffused magnets positioned at varying distances from the surface. There are two main types of areas, black and white areas, referring to the 2:14:1 phase and the RE-rich GB phase, respectively. After diffusion, the grain size is clearly smaller. Ramesh et al. (1988) derived the relationship between coercivity and grain size as $1/\ln D^n$, where D is the grain size. During GBDP, the melting RE-rich phase dissolves the bumps and corners of the main phases, thus reducing the size of the main grains. The finer the grains, the higher the Hcj of a magnet. The boundary in

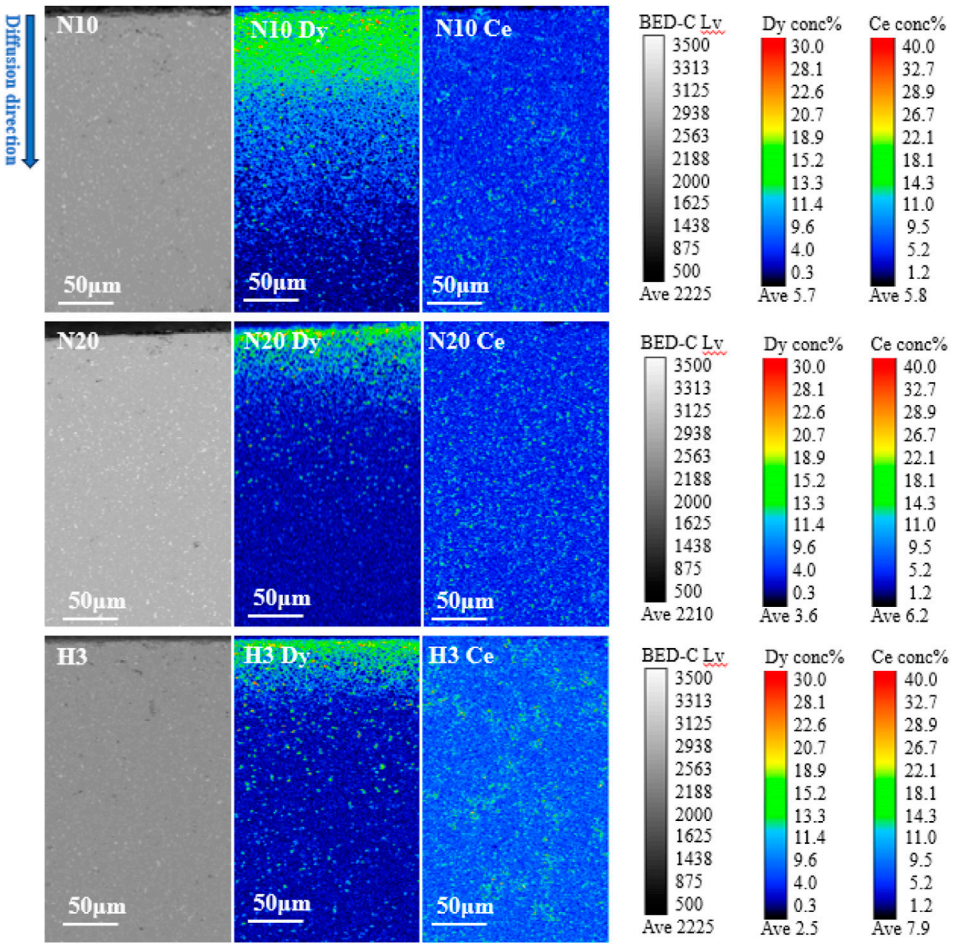

FIGURE 6
EPMA results for N20, N10, and H3 diffused samples.

the original magnet is blurred, which means that the matrix grains are not well-isolated. After diffusion, the grain boundaries are optimized and become clearer. Moreover, a Dy-rich core shell was observed in all diffused samples. At a distance of 50 μm from the magnet surface, the Dy-rich core shell is notable in all diffused samples. However, as the diffusion distance increases, the shells gradually become thinner. At a depth of 100 μm, the shells can hardly be observed in the N0 and N20 diffused samples, whereas they remain visible in the N10 diffused sample. This means that Dy is diffused deeper into the N10 diffused sample and Dy distribution is more uniform. On the contrary, for the N0 and H3 diffused samples, Dy seems consumed in the surface, and less Dy diffused deeper.

Figure 3 demonstrates the EDS mapping of diffused samples at a depth of 50 μm. Nd is enriched in the triple junctions (TJs). In contrast, Dy enriches around the matrix main phases and evenly enters the main phases. Dy will replace Pr or Nd with $(Pr/Nd)_2Fe_{14}B$ to form the $Dy_2Fe_{14}B$ phase (Liu et al., 2021). This explains the remanence decreases after the GBD process because the saturation magnetization (Js) for $Dy_2Fe_{14}B$ is lower than $(Pr/Nd)_2Fe_{14}B$. Furthermore, Ce is enriched in the TJs among all diffused magnets. According to Yan et al. (2014), Ce tends to enrich in the grain boundaries; when the Ce content is higher than 6.0 wt%, a $CeFe_2$ phase is formed at the intergranular boundary of the sintered Nd-Ce-Fe-B magnet. Too much $CeFe_2$ phase is harmful for the coercivity of the magnet because it deteriorates the wettability of grain boundary phases.

In order to reveal the coercivity enhancement and diffusion mechanism, the magnets were GBDP-treated by diffusing $Dy_{90}Al_{10}$ and $Nd_{10}Dy_{80}Al_{10}$ alloys. The diffusion heat-treatment is 1,213.2K/x h, followed with 923.2K/5 h (x = 1,2,3,4). EDS was conducted to measure the Dy and Nd concentrations at a depth of 100 μm from the surface of a diffused sample. Since the original magnets contain no Dy, all Dy in the magnets are diffused. In addition, the Nd concentration is deducted from the Nd content in the original magnet. The Nd and Dy concentrations as functions of heat-treatment time were examined, and the results are shown in Figure 4A. As diffusion time increases, Nd and Dy contents increase in all diffused samples. The Dy content of the $Nd_{10}Dy_{80}Al_{10}$ diffused sample is larger than that of the $Dy_{90}Al_{10}$ diffused sample. Figure 4B shows the concentration ratio Dy/Nd at GBs in the $Nd_{10}Dy_{80}Al_{10}$ diffused sample. At the first-step diffusion time of 1 h, the value is 6.21, which is lower than the atomic number ratio in $Nd_{10}Dy_{80}Al_{10}$ (8:1). For times of 2, 3, and 4 h, the Dy/Nd ratio decreases to 4.15, 3.42, and 2.92, respectively. This shows that the diffusion of Nd is faster than that of Dy, providing diffusion channels for subsequent Dy diffusion. This explains Dy is more uniform and

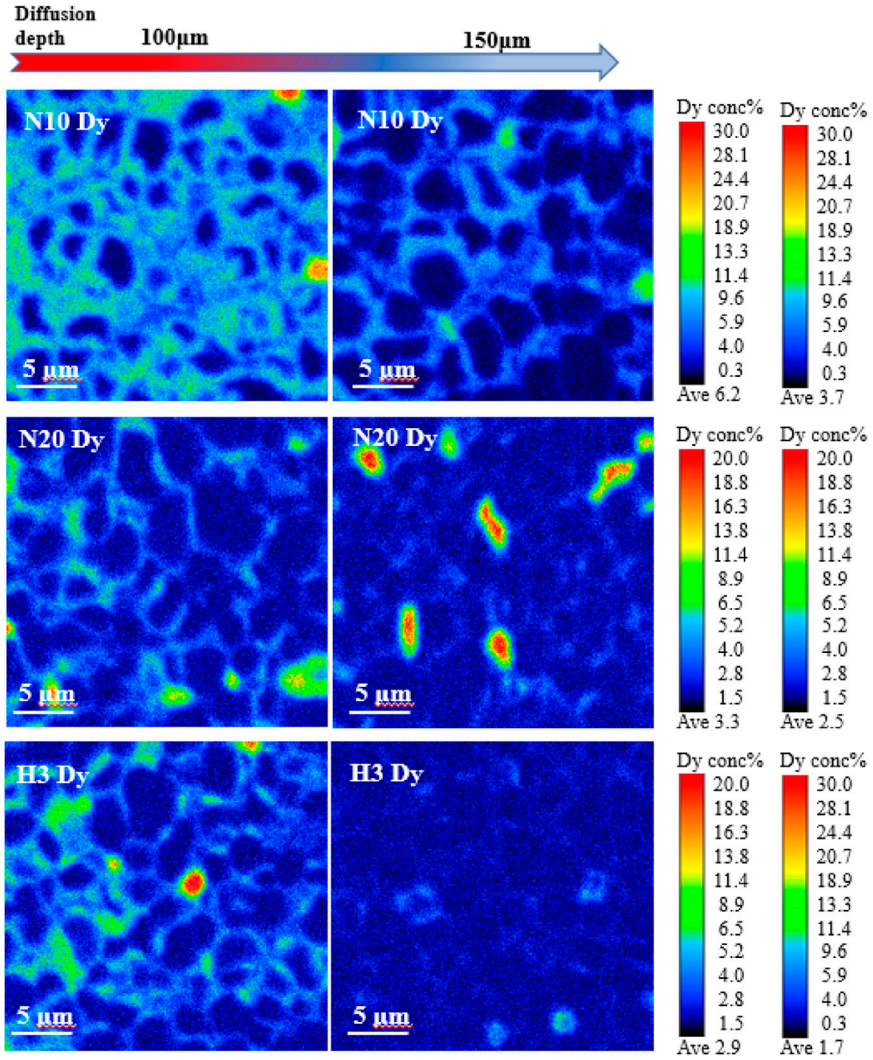

FIGURE 7
Dy distribution at different diffusion depths for N20, N10, and H3 diffused samples.

diffused deeper in the N10 diffused sample. According to Liu et al. (2018), an HRE-rich shell considerably increases coercivity due to the decoupling of matrix grains. The thinner and deeper the distribution of the HRE-rich shell, the higher coercivity and more homogeneously magnets can be obtained.

The original magnet contains 5% Ce, and SEM images show that there are two kinds of grain boundary phases in $Nd_{10}Dy_{80}Al_{10}$ diffused magnets (Figure 5), a gray grain boundary phase and a white grain boundary phase (Figure 5A1). In order to ascertain the components of the grain boundary phases in the $Nd_{10}Dy_{80}Al_{10}$ diffused sample, EDS line scanning was used (Figures 5A2–B5). Figures 5B3, B4 show that the ratio of Ce to Fe is 1:2 in the gray grain boundary. According to the results obtained by Zhang et al. (2017) and Xiong et al. (2018), there is a $CeFe_2$ phase in the original magnet. Figures 5A5, B5 show that, after diffusion, the Dy content in the gray grain boundary phase is higher than that in the white grain boundary phase, indicating that Dy is mostly consumed in the gray grain boundary phase. This observation suggests that Ce and Fe impede the diffusion of Dy, causing it to accumulate in the gray area. It is worth noting that the melting temperature of the metallic RE-rich phase is approximately 919.2 K (Zeng et al., 2019), which is lower than that of the $CeFe_2$ phase (1,198.2 K). The high melting point of $CeFe_2$ contributes to poor wettability in the gray region, hindering the diffusion of Dy and resulting in its accumulation within this region. This reduces the coercivity enhancement effect of Ce-containing magnets.

In order to explore the effect of Nd addition on the diffusion of Ce-containing Nd-Fe-B magnets, the EPMA measurements of the N10, N20, and H3 diffused samples were conducted (Figure 6). The Dy content in N10 and N20 is higher than H3, and the diffusion depth of Dy in N10 is significantly deeper than H3. This indicates that the addition of Nd is conducive to the diffusion of Dy in Ce-containing Nd-Fe-B. According to Tang et al. (2017), Nd can optimize the wettability of grain boundary phases. A contiguous grain boundary is beneficial for the diffusion of Dy. Therefore, the diffusion depth of Dy is deeper in N10 than that in H3. This is consistent with the previous discussion that the coercivity of the N10 diffused sample is higher than that of N0 and H3.

Figure 7 demonstrates the Dy distribution at the depth of 100 and 150 μm in the N10, N20, and H3 diffused samples. Dy is enriched

around the matrix main phases in all diffused samples. At the same diffusion depth, the Dy content in N10 is higher than that in N20 and H3. In addition, the Dy content in N20 is higher than that in H3. This indicates that more Dy is diffused into the magnet in Nd-containing diffusion. The Nd-containing diffusion source promotes the diffusion of Dy, which is beneficial to improve the coercivity of the magnet. The aforementioned work provides a method of the synergetic effects between Nd and Dy to develop the low-cost Nd-Ce-Fe-B magnets.

4 Conclusion

Coercivity enhancement of 5% wt Ce-containing Nd-Fe-B sintered magnets was achieved by diffusing $Nd_xDy_{90-x}Al_{10}$ alloys. The coercivity increased significantly from 1,124.7 to 1,656.4, 1,673.9, and 1,584.8 kA/m, for $Dy_{90}Al_{10}$, $Nd_{10}Dy_{80}Al_{10}$, and $Nd_{20}Dy_{70}Al_{10}$ samples, respectively. Although the Dy deposited in the $Nd_{10}Dy_{80}Al_{10}$ diffused sample was 0.8%wt of the original magnet, which is lower than that of the $Dy_{90}Al_{10}$ diffused sample (0.9%wt), its coercivity increment rate is significantly higher. The microstructure of the N10 diffused sample showed that the addition of Nd improved the distribution of grain boundary phases, which provides channels for subsequent Dy diffusion. In addition, a high melting point $CeFe_2$ phase was present in the Ce-containing Nd-Fe-B magnets, and significant amounts of Dy accumulated in this phase, resulting in Dy wastage. This situation was optimized using Nd-containing alloy as a diffusion source. Here, Dy could diffuse further due to the increased fluidity of the grain boundary phase by the addition of Nd.

Data availability statement

The original contributions presented in the study are included in the article/Supplementary Material; further inquiries can be directed to the corresponding author.

Author contributions

LL: conceptualization, data curation, investigation, supervision, writing–original manuscript, and writing–review and editing. RW: writing–review and editing. DC: writing–review and editing and data curation. RL: resources and writing–review and editing. PM: supervision and writing–review and editing. TW: formal analysis and writing–review and editing. HW: project administration and writing–review and editing.

Funding

The author(s) declare financial support was received for the research, authorship, and/or publication of this article. This work was supported by the National key scientific and technological project of China (Project No. E210E001010).

Conflict of interest

The authors declare that the research was conducted in the absence of any commercial or financial relationships that could be construed as a potential conflict of interest.

Publisher's note

All claims expressed in this article are solely those of the authors and do not necessarily represent those of their affiliated organizations, or those of the publisher, the editors, and the reviewers. Any product that may be evaluated in this article, or claim that may be made by its manufacturer, is not guaranteed or endorsed by the publisher.

References

Chen, F., Cong, M., Chen, H., Liu, N., Wang, D., Wang, X., et al. (2020). Coercivity enhancement of a Ce-based permanent magnet by grain boundary diffusion with Re70Cu30 (Re: Nd/Dy) eutectic alloys. *J. Alloys Compd.* 819, 152965. doi:10.1016/j.jallcom.2019.152965

Cui, X. G., Cui, C. Y., Cheng, X. N., and Xu, X. J. (2014). Effect of Dy_2O_3 intergranular addition on thermal stability and corrosion resistance of Nd–Fe–B magnets. *Intermetallic* 55, 118–122. doi:10.1016/j.intermet.2014.07.020

Di, J., Ding, G., Tang, X., Yang, X., Guo, S., Chen, R., et al. (2018). Highly efficient Tb-utilization in sintered Nd-Fe-B magnets by Al aided TbH_2 grain boundary diffusion. *Scr. Mater.* 155, 50–53. doi:10.1016/j.scriptamat.2018.06.020

Du, R., Chen, R., Ding, G., Fan, X., Tang, X., Cao, S., et al. (2022). Coercivity enhancement of the sintered Nd-Ce-Fe-B magnet via grain boundary diffusion with $Tb_{70}Fe_{30}$ alloy. *J. Magn. Magn. Mater.* 551, 169034. doi:10.1016/j.jmmm.2022.169034

Fan, X., Ding, G., Chen, K., Guo, S., You, C., Chen, R., et al. (2018). Whole process metallurgical behavior of the high-abundance rare-earth elements LRE (La, Ce and Y) and the magnetic performance of Nd0.75LRE0.25-Fe-B sintered magnets. *Acta Mater* 154, 343–354. doi:10.1016/j.actamat.2018.05.046

Jiang, C., He, J., Yu, Z., Cao, J., Song, W., Zhang, X., et al. (2022). Dy-based dual-alloy grain boundary diffusion for sintered Nd-Fe-B magnets with improved magnetic performance and corrosion resistance. *Mater. Charact.* 193, 112319. doi:10.1016/j.matchar.2022.112319

Li, Z., Yao, K. F., Liu, T. C., Li, X., and Wang, S. (2022). Effect of annealing on the magnetic properties of FeCoNiCuNbSiB soft magnetic alloys. *Front. Mater.* 8, 805609. doi:10.3389/fmats.2021.805609

Liang, L., Ma, T., Zhang, P., Jin, J., and Yan, M. (2014). Coercivity enhancement of NdFeB sintered magnets by low melting point $Dy_{32.5}Fe_{62}Cu_{5.5}$ alloy modification. *J. Magn. Magn. Mater.* 355, 131–135. doi:10.1016/j.jmmm.2013.11.007

Liu, L., Sepehri-Amin, H., Sasaki, T. T., Ohkubo, T., Yano, M., Sakuma, N., et al. (2018). Coercivity enhancement of Nd-Fe-B hot-deformed magnets by the eutectic grain boundary diffusion process using Nd-Ga-Cu and Nd-Fe-Ga-Cu alloys. *AIP Adv.* 8, 056205. doi:10.1063/1.5006575

Liu, R., Qu, P., Zhou, T., Pan, W., Li, M., Huang, Q., et al. (2021). The diffusion behavior and striking coercivity enhancement by Dip-coating TbH_3 powders in sintered NdFeB magnets. *J. Magn. Magn. Mater.* 536, 168091. doi:10.1016/j.jmmm.2021.168091

Liu, X., Zhang, Y., Zhang, P., Ma, T., Yan, M., Zhao, L., et al. (2019). Microstructure evolution of $Dy_{69}Ni_{31}$-added Nd-Fe-B sintered magnets during annealing. *J. Magn. Magn. Mater.* 486, 165260. doi:10.1016/j.jmmm.2019.165260

Lu, K., Bao, X., Tang, M., Chen, G., Mu, X., Li, J., et al. (2017). Boundary optimization and coercivity enhancement of high (BH) max Nd-Fe-B magnet by diffusing Pr-Tb-Cu-Al alloys. *Scr. Mater.* 138, 83–87. doi:10.1016/j.scriptamat.2017.05.048

Ramesh, R., Thomas, G., and Ma, B. M. (1988). Magnetization reversal in nucleation-controlled magnets. II. Effect of grain size and size distribution on intrinsic coercivity of Fe-Nd-B magnets. *J. Appl. Phys.* 64, 6416–6423. doi:10.1063/1.342055

Sepehri-Amin, H., Ohkubo, T., and Hono, K. (2013). The mechanism of coercivity enhancement by the grain boundary diffusion process of Nd–Fe–B sintered magnets. *Acta Mater* 61, 1982–1990. doi:10.1016/j.actamat.2012.12.018

Shi, Q., Liu, Y., Li, J., Zhao, W., Wang, R., and Gao, X. (2019). Significant improvement of the 2:14:1 phase formability and magnetic properties of multi-

phases RE-Fe-B magnets with La substitution for Ce. *J. Magn. Magn. Mater.* 476, 1–6. doi:10.1016/j.jmmm.2018.12.043

Takezawa, M., Taneda, H., and Morimoto, Y. (2015). Relationship between microstructure and magnetic domain structure of Nd-Fe-B melt-spun ribbon magnets. *Front. Mater. Sci.* 9, 206–210. doi:10.1007/s11706-015-0297-5

Tang, M., Bao, X., Lu, K., Sun, L., Mu, X., Li, J., et al. (2017). Microstructure modification and coercivity enhancement of Nd-Ce-Fe-B sintered magnets by grain boundary diffusing Nd-Dy-Al alloy. *J. Magn. Magn. Mater.* 442, 338–342. doi:10.1016/j.jmmm.2017.06.116

Wang, J., Wang, G., and Zeng, D. (2020). Coercivity and corrosion resistance enhancement of multi-main-phase Nd-Ce-Fe-B sintered magnets by the grain boundary diffusion process using $Pr_{81.5}Ga_{19.5}$ and $Pr_{81.5}Ga_{14.5}Cu_5$ alloys. *J. Magn. Magn. Mater.* 503, 166639. doi:10.1016/j.jmmm.2020.166639

Xiong, J. F., Shang, R. X., Liu, Y. L., Zhao, X., Zuo, W. L., Hu, F. X., et al. (2018). Magnetic properties of misch-metal partially substituted Nd–Fe–B magnets sintered by dual alloy method. *Chin. Phys. B* 27, 077504. doi:10.1088/1674-1056/27/7/077504

Yan, C., Guo, S., Chen, R., Lee, D., and Yan, A. (2014). Enhanced magnetic properties of sintered Ce–Fe–B-based magnets by optimizing the microstructure of strip-casting alloys. *IEEE Trans. Magn.* 50, 1–4. doi:10.1109/TMAG.2014.2325404

Zeng, H., Liu, Z., Li, W., Zhang, J., Zhao, L., Zhong, X., et al. (2019b). Significantly enhancing the coercivity of NdFeB magnets by ternary Pr-Al-Cu alloys diffusion and understanding the elements diffusion behavior. *J. Magn. Magn. Mater.* 471, 97–104. doi:10.1016/j.jmmm.2018.09.080

Zeng, H. X., Liu, Z. W., Zhang, J. S., Liao, X. F., and Yu, H. Y. (2020). Towards the diffusion source cost reduction for NdFeB grain boundary diffusion process. *J. Mater. Sci. Technol.* 36, 50–54. doi:10.1016/j.jmst.2019.08.009

Zeng, H. X., Yu, H. Y., Zhou, Q., Zhang, J. S., Liao, X. F., and Liu, Z. W. (2019a). Clarifying the effects of La and Ce in the grain boundary diffusion sources on sintered NdFeB magnets. *Mater. Res. Express.* 6, 106105. doi:10.1088/2053-1591/ab3756

Zhang, L., Zhu, M., Song, L., Liu, T., Fang, Y., Guo, Y., et al. (2019). The technology and mechanism of coercivity promotion of Ce-rich dual-main-phase sintered magnets. *J. Magn. Magn. Mater.* 490, 165414. doi:10.1016/j.jmmm.2019.165414

Zhang, Y., Ma, T., Jin, J., Li, J., Wu, C., Shen, B., et al. (2017). Effects of $REFe_2$ on microstructure and magnetic properties of Nd-Ce-Fe-B sintered magnets. *Acta Mater* 128, 22–30. doi:10.1016/j.actamat.2017.02.002

Zhou, T., Chen, J., Wang, Q., Pan, W., Huang, Q., Liu, R., et al. (2023). Super-high coercivity NdFeB magnet fabricated with double Tb-rich/lean shells by double alloy method and grain boundary diffusion. *J. Alloys Compd.* 937, 168368. doi:10.1016/j.jallcom.2022.168368

Zhu, J., Ding, G., Zheng, B., Wu, H., Jin, L., Jin, Z., et al. (2022). Effects of Pr-Cu-Ti intergranular addition on microstructure and magnetic properties of heavy-rare-earth-free Nd-Fe-B sintered magnets. *J. Rare Earths* 40, 778–783. doi:10.1016/j.jre.2021.02.007

Zhu, M., Li, W., Wang, J., Zheng, L., Li, Y., Zhang, K., et al. (2014). Influence of Ce content on the rectangularity of demagnetization curves and magnetic properties of Re-Fe-B magnets sintered by double main phase alloy method. *IEEE Trans. Magn.* 50, 1–4. doi:10.1109/TMAG.2013.2278018